Accuracy of ab initio electron correlation and electron densities in vanadium dioxide

Ilkka Kylänpää, Janakiraman Balachandran, Panchapakesan Ganesh, Olle Heinonen, Paul R. C. Kent, and Jaron T. Krogel

Phys. Rev. Materials **1**, 065408 — Published 27 November 2017

DOI: 10.1103/PhysRevMaterials.1.065408

Accuracy of *ab initio* electron correlation and electron densities in vanadium dioxide*

Ilkka Kylänpää[1],† Janakiraman Balachandran[2], Panchapakesan Ganesh[2], Olle Heinonen[3,4], Paul R. C. Kent[2,5], and Jaron T. Krogel[1]

[1] *Materials Science and Technology Division, Oak Ridge National Laboratory, Oak Ridge, Tennessee 37831, USA*
[2] *Center for Nanophase Materials Sciences, Oak Ridge National Laboratory, Oak Ridge, Tennessee 37831, USA*
[3] *Materials Science Division, Argonne National Laboratory, Lemont, Illinois 60439, USA*
[4] *Center for Hierarchical Material Design, Northwestern-Argonne Institute for Science and Engineering, Northwestern University, Evanston, Illinois 60208, USA and*
[5] *Computational Sciences and Engineering Division, Oak Ridge National Laboratory, Oak Ridge, Tennessee 37831, USA*

(Dated: October 31, 2017)

Diffusion quantum Monte Carlo results are used as a reference to analyze properties related to phase stability and magnetism in vanadium dioxide computed with various formulations of density functional theory. We introduce metrics related to energetics, electron densities and spin densities that give us insight on both local and global variations in the antiferromagnetic M1 and R phases. Importantly, these metrics can address contributions arising from the challenging description of the 3d orbital physics in this material. We observe that the best description of energetics between the structural phases does not correspond to the best accuracy in the charge density, which is consistent with observations made recently by Medvedev et al. [Science 355, 49 (2017)] in the context of isolated atoms. However, we do find evidence that an accurate spin density connects to correct energetic ordering of different magnetic states in VO_2, although local, semilocal, and meta-GGA functionals tend to erroneously favor demagnetization of the vanadium sites. The recently developed SCAN functional stands out as remaining nearly balanced in terms of magnetization across the M1-R transition and correctly predicting the ground state crystal structure. In addition to ranking current density functionals, our reference energies and densities serve as important benchmarks for future functional development. With our reference data, the accuracy of both the energy and the electron density can be monitored simultaneously, which is useful for functional development. So far, this kind of detailed high accuracy reference data for correlated materials has been absent from the literature.

I. INTRODUCTION

Due to their unique and controllable properties, functional materials are at the forefront of novel device applications and condensed matter physics. For example, in the strongly correlated electron material vanadium dioxide (VO_2) one such property is a thermally induced metal to insulator transition (MIT) which is accompanied by a change in the underlying crystal lattice structure. In addition to temperature, a variety of techniques have been devised to control the MIT in VO_2, such as photoexcitation, hydrostatic pressure, unaxial stress and electrical gating[1–8], opening the door to a range of possible device applications.

At ambient pressure, the MIT occurs at $T_c \approx 341$ K for pure unstrained VO_2. Below T_c unstrained VO_2 is in an insulating monoclinic phase (M1), and above T_c it is stable in a metallic rutile phase (R)[9–11]. The mechanism for the temperature driven transition between these two phases is not yet fully resolved, with recent studies favoring strong electron-electron correlations, Peierls-type transition, or the coexistence of both[12–16]. For example, very recent Hubbard model calculations would indicate that the Mott mechanism is the dominant feature[17] while a phonon study would indicate a Peierls-type transition[8]. *Ab initio* quantum Monte Carlo (QMC) studies demonstrate that an accurate account of electron correlations is crucial to predict the electronic and magnetic properties of VO_2 across the phase transition[18].

Experimental studies are today often accompanied with density functional theory (DFT)[19,20] calculations for better understanding, and DFT calculations have been used in isolation to provide insight into the underlying mechanisms of the VO_2 monoclinic to rutile phase transition[1,2,21–23]. However, the main challenges with DFT approaches relate to a consistent and accurate account of electronic correlation, and the calculated properties may vary rather substantially depending on the chosen exchange-correlation functional. A recent comprehensive study of DFT functionals[24] applied to atoms noted that functional development has strayed in recent years from the focus on obtaining accurate densities in favor of reaching better energetics by empirical means. From this point of view progress in DFT functionals would improve both the energy and density, with these improvements clearly visible when compared with accurate benchmark data. High quality benchmark studies of this type are rare in the solid state and more especially in regard to highly correlated oxides such as VO_2. In this regard a benchmark quality study of these properties in VO_2 is timely.

To this end, we will utilize quantum Monte Carlo methodology, and diffusion Monte Carlo (DMC)[25] in particular, which is known for its accuracy in solving ground state electronic structure properties for both molecular and solid state systems from first principles[18,25–28]. In

practice the main advantage of the DMC approach is its accurate and straightforward account of electron correlations[29,30]. Calculations of transition metal oxides (TMOs) are challenging due to the description of correlated electrons, in particular, the localization and correlation related to 3d orbitals. However, successful application of DMC to TMOs is now well established by excellent agreement with experimental data, e.g., in properties such as lattice constants, cohesive/formation energies, and magnetic excitations[31–42]. Applications in this domain are nevertheless fairly recent, as expansions in computational power and improvements in QMC codes have enabled such studies to be performed in just the last few years.

Our main focus is directed on the differences in the DMC and DFT in describing the antiferromagnetic (AFM) M1 and R phases of vanadium dioxide. This magnetic structure is chosen because it is the lowest energy state identified so far in the M1 phase and it is nearly degenerate with other candidate magnetic structures in the R phase[18]. We concentrate on variations in energetics, electron densities, and electronic spin densities to address phase stability and magnetism. The metrics introduced in this work enable us to consider the differences in both local and global properties of the studied system and rank current density functionals accordingly by property. This ranking may be of interest to DFT practitioners to guide functional selection when fidelity to a single property (e.g. phase stability or magnetism) is most relevant, or if a reasonable balance of quality among properties is sought. Since the most relevant physics (relating to the 3d orbitals) is common to many transition metal oxides, we expect our conclusions to transfer to other materials. In addition to ranking density functionals, our reference energetics, charge and spin densities serve as important benchmarks for future functional development aimed at correlated materials.

II. METHODS AND METRICS

We have obtained energies, electron densities and spin densities for AFM M1 and R phases of VO_2 with quantum Monte Carlo (QMC), i.e., variational Monte Carlo (VMC) and DMC, as well as with DFT. The range of DFT functionals employed include those from the first four rungs of "Jacob's ladder": local functionals (LDA[43]), semi-local functionals (PBE[44,45], PBEsol[46,47]), meta-GGA's (TPSS[48], SCAN[49,50]), and hybrid functionals (PBE0[51], HSE[52,53]). We also consider Hubbard-corrected local (LDA+U[54]) and semi-local (PBE+U) functionals. The reference calculations with DMC and a subset of DFT results use our hard norm conserving RRKJ[55] (OPT) pseudopotentials. Since the exact functional does not depend on the external potential[19], by keeping the pseudopotential fixed we can better compare local differences in DMC and DFT total and spin densities. Additionally, we have performed DFT calculations using VASP[56–59] with projector augmented wave (PAW) potentials[60,61], and Quantum Espresso (QE)[62] with ultrasoft GBRV-potentials[63], which can be used in comparing the formation energy (R-M1 energy difference) and magnetization. The results with PAW and ultrasoft pseudopotentials are labeled by " * " (VASP-PAW) and " † " (QE-GBRV) throughout the article. The Nexus interface[64] was used in the creation and execution of all simulation workflows.

Crystal structures for the M1[65] and R[66] phases were obtained from the Inorganic Crystal Structure Database[67]. All calculations were performed with the experimental lattice constants. In both phases, the vanadium atoms are arranged in quasi-1D chains and, as in Ref.[18], an antiferromagnetic ordering was imposed by fixing alternating up/down spin moments along the chains. More detail on the experimental lattice vectors and atomic coordinates of the M1 and R crystal structures are provided in the supplemental material[68].

QMC simulations were carried out with QMCPACK[69] in a supercell containing 16 VO_2 formula units. For faster convergence to thermodynamic limit, we used twist-averaged boundary conditions[70] with a $3\times3\times3$ supercell twist angle grid instead of purely periodic boundary conditions. The trial wavefunction (Ψ_T) used is of the standard Slater-Jastrow[71,72] type:

$$\Psi_T = \det\{\psi_\uparrow\}\det\{\psi_\downarrow\}e^J. \quad (1)$$

The purpose of the trial wavefunction is to guide the simulation both more accurately and more rapidly to the ground state. A trial wavefunction with a better nodal surface–arising from the sets of orbitals above–leads to a more accurate DMC result. A trial wavefunction with a better Jastrow factor improves the timestep and pseudopotential localization approximations made in DMC and also reduces the statistical variance, making the calculations more efficient. Since a good trial wavefunction is important in improving the approximations made in DMC, we describe in more detail below how we obtained an optimal wavefunction within the Slater-Jastrow ansatz.

The product of spin-up and spin-down determinants of spatial orbitals arise from a single determinant of spin-orbitals after fixing the electron spins, while the overall state is a spin-unrestricted antiferromagnet[33]. The determinants are composed of single particle orbitals taken from spin-unrestricted LDA+U (via Quantum Espresso), in which the correct magnetic structure was imposed by initializing the magnetic moments in an antiferromagnetic configuration along the V-V chains. Convergence to the AFM state was further confirmed after the self-consistent density functional theory calculations by analysis of the magnetic structure and spin-resolved Löwdin charges.

In the Jastrow factor (e^J) we include terms up to three-

body (electron-electron-ion) correlation functions, i.e.,

$$\begin{aligned} J =& J_1 + J_2 + J_3 \\ =& \sum_{I,i} u_1(|r_i - R_I|) + \sum_{i<j} u_2(|r_i - r_j|) \\ &+ \sum_{I,i<j} u_3(|r_i - r_j|, |r_i - R_I|, |r_j - R_I|) \end{aligned} \quad (2)$$

where r_i and R_I refer to electron and ion coordinates, respectively. The u_1, u_2, and u_3 correlation functions depend, as appropriate, on both the ionic and spin species involved. These functions are parameterized in terms of radial B-splines in the case of u_1/u_2 and as a product of low order polynomials in the case of u_3[73].

The Jastrow parameters were optimized by making use of the variational principle as applied to the total energy and the energy variance. The optimization was performed by minimizing a cost function containing a 95/5 ratio of energy and variance with the linear method[74], which results in a good balance between improvements in DMC pseudopotential localization approximation[75–77] and the resulting variance of the local energy[78]. We optimize the Jastrow part only with VMC, which improves the description of particle-particle correlations, but does not modify the nodal surface. The orbitals are instead optimized directly with DMC, though within the restricted variational freedom afforded by LDA+U.

In DMC the operator $\exp[-\tau(\hat{H} - E_T)]$ is used to project out the lowest eigenstate that has non-zero overlap with the chosen fixed node / trial wave function[25], where $\hat{H}$ is the many body Hamiltonian and E_T is an estimate of the ground state energy, which is updated throughout the simulation. The DMC fixed node/phase error[79–81] was minimized by using the Hubbard-U value as a variational parameter optimized directly in DMC, with $U = 3.5$ eV yielding the lowest energy, which is demonstrated in the supplemental material. In production runs, the DMC timestep was set to 0.005 Ha^{-1}, resulting in an acceptance ratio greater than 99.6%. Nonlocal pseudopotentials were handled in the DMC projector within the variational T-moves scheme[77,82].

In general, our DFT calculations were performed in the AFM magnetic primitive cell of VO_2 (4 VO_2 formula units for M1 or R) using a $6\times6\times6$ k-space grid and plane-wave energy cutoffs of 350 Ry (OPT-potentials), 300 Ry (GBRV-potentials), and 500 eV (VASP PAW-potentials). For Quantum Espresso calculations involving meta-GGA (TPSS) and hybrid functionals (PBE0, HSE), somewhat coarser k-point grids and energy cutoffs had to be used to reduce cost, though in all cases we estimate the expected error to be 1 meV per formula unit or less. The convergence studies mentioned above are described in more detail in the supplemental material. Full simulation inputs and outputs for all QMC and DFT calculations performed in this work are available via the Materials Data Facility[83] (DOI: provided upon acceptance).

Since DMC provides a "mixed" estimate of the density (a mixture between the fixed node density and the VMC one), we have corrected the mixed estimates by extrapolation to obtain "pure" estimates of the density, reflecting the fixed node wave function (Φ) alone. This is a general property of the DMC method for operators that do not commute with the Hamiltonian. In order to obtain pure estimates of the density, two extrapolation formulas have been used[25]:

$$\rho_1 = 2\rho_{\mathrm{DMC,mixed}} - \rho_{\mathrm{VMC}} + \mathcal{O}((\Phi - \Psi_T)^2) \quad (3)$$

$$\rho_2 = \frac{\rho^2_{\mathrm{DMC,mixed}}}{\rho_{\mathrm{VMC}}} + \mathcal{O}((\Phi - \Psi_T)^2). \quad (4)$$

In practice, we have found that the two estimates yield the same densities to a high degree of accuracy, consistent with fully purified densities, and thus we report values using Eq. (3) only. Our benchmark extrapolated DMC total and spin densities are available in the supplemental material[68].

In order to quantify the errors incurred by the various DFT functionals, we define a set of metrics that enable us to assess both local and global variations from our accurate reference. To compare functionals in terms of energetics we use the R/M1 energy difference ($\Delta E \equiv E_{\mathrm{R}} - E_{\mathrm{M1}}$)

$$\delta E = \Delta E - \Delta E_{\mathrm{DMC}}, \quad (5)$$

and for densities we use the root-mean-square (RMS) deviation of the total density (ρ_{tot}) and spin density ($\rho_{\mathrm{spin}} = \rho^{\uparrow} - \rho^{\downarrow}$) over the unit cell

$$\mathrm{RMS}(\Delta\rho) = \left[\int (\rho - \rho_{\mathrm{DMC}})^2 dV/V\right]^{1/2}. \quad (6)$$

We also compare DFT and DMC using a global quantity related to the spin density (the "absolute magnetization")

$$M = \int |\rho^{\uparrow} - \rho^{\downarrow}| dV, \quad (7)$$

and the spherically averaged difference of total or spin densities about vanadium atoms

$$\rho_{\mathrm{avg}} = 4\pi r^2 \frac{\int d\Omega |\rho(r,\Omega)|}{\int d\Omega}. \quad (8)$$

These metrics allow us to rank density functionals on the basis of the quality of the two quantities fundamental to DFT, and also to gain insight into the magnetic behavior at the correlated V sites across the metal-insulator (R-M1) transition.

III. RESULTS

We focus mainly on properties relevant to the structural phase stability and magnetism of VO_2. We examine the quality of DFT descriptions of structural phase

stability by comparing the zero temperature R/M1 total energy differences obtained from DFT with our DMC benchmarks (Eq. 5). Also included in this section are comparisons of DFT total densities with DMC (Eqs. 6 and 8). DFT descriptions of magnetism are judged mainly on the basis of the spin density (Eqs. 6 and 8), including the absolute magnetization per VO_2 unit cell (Eq. 7). Moreover, related to magnetic properties we perform a spin gap study as a function of U, demonstrating a link between the quality of spin densities and the computed spin gap.

A. Phase stability

In Table I we consider the per formula unit energy difference between R and M1 phases of antiferromagnetic VO_2 obtained with various theoretical methods. All values are reported relative to our DMC estimate of $E_R - E_{M1} = 8(3)$ meV, which agrees very well with the DMC value previously obtained by Zheng and Wagner (10(6) meV)[18]. This study used different choices for the pseudopotentials and underlying basis set for the QMC wavefunctions, giving confidence in the DMC simulation methodology. The DFT functionals show a systematic bias toward incorrectly identifying the R phase as the ground state structure. Other than DMC, only four approaches correctly identify the M1 phase as the ground state: PBE, TPSS, SCAN*, and LDA+U ($U = 1.0$ eV).

TABLE I. Ranking of the functionals based on the energy difference between R and M1 phases: $\Delta E = E_R - E_{M1}$, and $\delta E = \Delta E - \Delta E_{DMC}$. Results are ranked first by the correct identification of the ground state structure (M1), and then by the absolute value of the δE error metric. Energies are given in meV/VO_2, and the 1-σ statistical error of DMC is 3 meV/VO_2, which provides the uncertainty for the differences. Listed U-values for LDA+U and PBE+U are in eV. Values obtained with PAW (VASP) and ultrasoft (Quantum Espresso) pseudopotentials are labeled as " * " or " † ", respectively. Point of "chemical accuracy" ($\sim$ 43.4 meV) is indicated by the horizontal line after the 16th rank.

Rank	Method	δE	Ground state
1.	DMC	0(3)	M1
2.	LDA+U(1.0)	−3(3)	M1
3.	PBE	−3(3)	M1
4.	TPSS	5(3)	M1
5.	SCAN*	28(3)	M1
6.	VMC	−19(3)	R
7.	LDA+U(2.0)	−23(3)	R
8.	PBE†	−28(3)	R
9.	TPSS*	−29(3)	R
10.	HSE	−29(3)	R
11.	PBEsol	−29(3)	R
12.	PBE0	−31(3)	R
13.	LDA†	−33(3)	R
14.	PBEsol†	−34(3)	R
15.	LDA	−34(3)	R
16.	LDA+U(1.0)†	−38(3)	R
17.	PBE*	−49(3)	R
18.	LDA+U(3.5)	−96(3)	R
19.	PBE+U(3.5)*	−127(3)	R
20.	PBE+U(4.0)*	−148(3)	R
21.	LDA+U(6.0)	−190(3)	R

In the case of VO_2, we do not see a systematic improvement in energetics as we ascend the "Jacob's ladder" of functionals. Strictly within calculations made with our norm conserving pseudopotentials, we find that semilocal (PBE) and meta-GGA (TPSS) functionals perform the best ($\delta E \sim 4$ meV) with local (LDA) and hybrids (PBE0, HSE) performing worse ($\delta E \sim 32$ meV). Despite this, nearly all functionals appear to experience a very large cancellation of error between the M1 and R phases, bringing the energy difference within the widely used reference of "chemical accuracy" (defined as 1 kcal/mol $\approx$ 43.4 meV)[84,85] relative to the DMC benchmark value. In this light, the various density functional approximations are actually performing quite well–when provided with the lowest energy magnetic structure (AFM)–as even simple functionals are "chemically accurate". The level of error cancellation observed here is most likely fortuitous, as *e.g.* hybrid functionals have been shown to deviate by $\sim 0.5 - 1.0$ eV from DMC benchmarks in other contexts such as cohesive energies and defect formation energies in other transition metal oxides[40,86–88]. The results that fall decidedly out of the range of chemical accuracy belong to Hubbard-corrected functionals including the U range (3.5-5.0 eV) identified by DMC as having an optimal –and therefore ostensibly physical– orbital structure. As we see in the next subsection, the physics reflected in this range of Hubbard U's relates more to the magnetic properties of VO_2.

The relevant energy scale in the VO_2 M1/R transition is sufficiently small that sources of systematic error other than the choice of functional also become relevant. Some of the DFT results, such as for PBE and TPSS, show sensitivity to pseudopotential details on the order of $21 - 46$ meV even where significant care has been given to their construction. For example, with the PBE functional the formation energy with PAW and GBRV pseudopotentials deviates from the one obtained using the OPT-potential by 46 meV and 25 meV, respectively, while the difference between PAW and GBRV is 21 meV with PBE.

When considering the total electronic density, we only reference the norm conserving (OPT) pseudopotentials for a sound comparison. In Table II we provide a ranking of the theoretical methods based on the root-mean-squared metric of the total electron density according to Eq. (6): RMS($\Delta\rho$) with ($\Delta\rho = \rho_{tot}^{Method} - \rho_{tot}^{DMC}$). In both the M1 and R phases, the Hubbard corrected LDA functional (with U in the $2 - 6$ eV range) performs the best in terms of overall accuracy of the electron density. Also in both phases, hybrid functionals (PBE0, HSE) perform better than the local (pure LDA) and semi-local (PBE, PBEsol) functionals, consistent with systematic improvements in the hybrids. The meta-

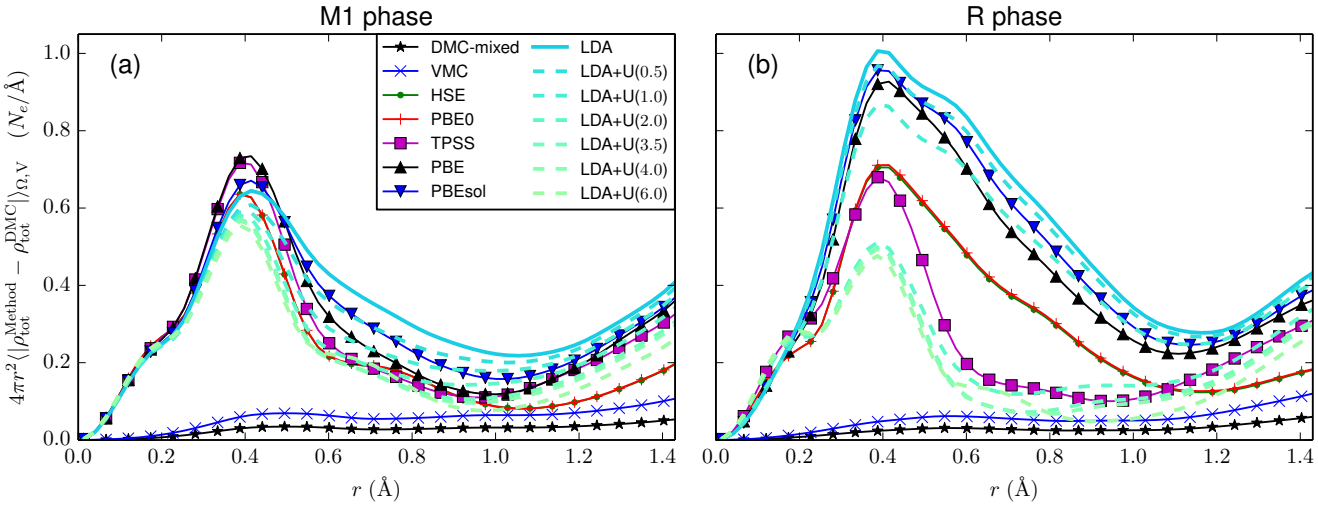

FIG. 1. Radial distribution function of absolute total density difference from extrapolated DMC (Eq. 8) around V atom for various theoretical methods using RRKJ pseudopotentials: (a) M1 phase, and (b) R phase. As a function of increasing U value the LDA+U density tends to an improved accuracy, i.e., as U is increased LDA+U curves get closer to zero.

GGA functional TPSS gives a mixed performance: it is among the worst in the M1 phase, but in the R phase it is significantly better than the hybrids in terms of the density. Even among the best performing functionals there is still considerable room for improvement as the level of accuracy afforded by an approximate three body Jastrow factor in VMC is roughly six times better, *i.e.* $\mathrm{RMS}(\Delta\rho_{\rm DFT})/\mathrm{RMS}(\Delta\rho_{\rm VMC}) \gtrsim 6$.

Looking across the M1 to R transition, most functionals (excepting LDA+U and TPSS) perform significantly worse in terms of the density in the R phase than for M1, though this bears little discernible relationship to the performance of the functionals in terms of energetics. In Fig. 1 we show spatial variations in the electron density with respect to DMC according to Eq. (8). We concentrate on a spherical region around one vanadium atom up to $r = 1.43$Å, and provide the radial distribution function of the absolute density difference. Here it should be emphasized that in the M1 phase there are two inequivalent V atoms, but for roughly $r < 1.9$Å there are no discernible differences in the radial metric. In both phases the density errors tend to peak where the density itself is also the highest: near the peak of the d-orbitals. This clear "bump" in the radial error distributions demonstrates that the DFT functionals are in general not capturing the $3d$ orbital well. A small $3d$ error is also very weakly present in VMC and DMC-mixed curves, which shows the effect of the more accurate extrapolated estimator. It should be noted that for an exact input trial wave function both VMC and DMC-mixed curves would collapse to zero. For reference, the non-local cutoff radius of our norm-conserving V pseudopotential is at 0.42Å, which is also near the d-peak.

TABLE II. Ranking based on the RMS deviation of the total electron density from extrapolated DMC according to Eq. (6): $\mathrm{RMS}(\Delta\rho)$ with $\Delta\rho = \rho_{\rm tot}^{\rm Method} - \rho_{\rm tot}^{\rm DMC}$. DMC-extrap refers to the most accurate evaluation of an observable from diffusion Monte Carlo (extrapolated estimate of Eq. 3), and is used as a reference. Density deviations are given in units of $N_e/\text{Å}^3$.

	M1 phase		R phase	
Rank	Method	$\mathrm{RMS}(\Delta\rho)$	Method	$\mathrm{RMS}(\Delta\rho)$
1.	DMC-extrap	0.000	DMC-extrap	0.000
2.	DMC-mixed	0.004	DMC-mixed	0.004
3.	VMC	0.009	VMC	0.008
4.	LDA+U$(2-6)$	0.061	LDA+U$(2-6)$	0.054
5.	LDA+U(1.0)	0.062	TPSS	0.063
6.	PBE0	0.064	HSE	0.068
7.	HSE	0.064	PBE0	0.068
8.	PBEsol	0.068	LDA+U(1.0)	0.081
9.	LDA	0.068	PBE	0.085
10.	TPSS	0.068	PBEsol	0.087
11.	PBE	0.071	LDA	0.092

Despite LDA+U(1.0eV) and PBE being ranked as second and third in terms of energetics (see Table I) they do not excel in density metrics around the V atom. Consistent with the global RMS density metric in Table II, the variations are noticeably increased by going from M1 phase to R phase. Within this transition it seems that only LDA+U with the larger U-values ($U \geq 2.0$ eV) as well as TPSS tend to maintain or even slightly improve the accuracy across the M1 to R transition. However, apart from TPSS these are ranked rather poorly in terms of the energy difference between the two phases.

B. Magnetism

An accurate description of magnetism is essential to obtain a correct account of the structural phase stability in VO_2. As has been shown in prior DFT studies[22,89], the calculated energy differences between different magnetic configurations in a single structural phase can be larger than the expected enthalpy of formation based on experiment. It is therefore pertinent to explore the magnetic properties of the various functionals, as represented by the spin density, relative to our DMC benchmarks. As before, we consider the AFM state, which is the lowest energy state observed so far in the M1 phase and which is effectively degenerate with other magnetic states in the paramagnetic R phase according to recent DMC calculations[18].

In Table III we provide the ranking related to accuracy in electronic spin density by the root-mean-squared metric of $\Delta\rho = \rho_{\rm spin}^{\rm Method} - \rho_{\rm spin}^{\rm DMC}$. Based on the results, the density functionals considered are generally more accurate in their description of the spin density than the total density. For the most accurate functionals, the observed errors are only about $2-3\times$ greater than VMC versus the factor of six observed for the total density. Overall the DMC optimized LDA+U functional ($U = 3.5$ eV) performs substantially better than the others, indicating that the optimal U–in terms of the DMC energy–is being selected based on the correct description of local magnetic moments. In the M1 phase, improvements to the spin density exactly follow the expected progression with the errors following LDA>PBE>TPSS>HSE. Crossing the transition to the metallic R phase, this ordering is largely preserved but with the hybrids now lagging behind meta-GGA. Local, semilocal, and hybrid functionals all experience a large increase in the spin density error in the R phase relative to M1, while for LDA+U(3.5) and TPSS the density errors remain unaffected by the structural transition. The source of these large differences is purely angular in nature as can be seen by inspecting the local magnetic moments and the angularly sensitive radial error metric of Eq. (8) (see supplemental material Figs. 6 and 7).

TABLE III. Ranking related to description of magnetism. The ranking is based on the RMS deviation of the spin density from extrapolated DMC according to Eq. (6): RMS($\Delta\rho$) with $\Delta\rho = \rho_{\rm spin}^{\rm Method} - \rho_{\rm spin}^{\rm DMC}$. Spin density deviations are given in units of $N_e/\text{Å}^3$.

	M1 phase		R phase	
Rank	Method	RMS($\Delta\rho_{\rm spin}$)	Method	RMS($\Delta\rho_{\rm spin}$)
1.	DMC-extrap	0.000	DMC-extrap	0.000
2.	DMC-mixed	0.003	DMC-mixed	0.003
3.	VMC	0.006	VMC	0.007
4.	LDA+U(3.5)	0.016	LDA+U(3.5)	0.015
5.	PBE0	0.022	LDA+U(2.0)	0.016
6.	HSE	0.022	TPSS	0.019
7.	LDA+U(2.0)	0.022	LDA+U(6.0)	0.020
8.	LDA+U(6.0)	0.024	HSE	0.049
9.	TPSS	0.024	PBE0	0.050
10.	PBE	0.039	PBE	0.073
11.	LDA+U(1.0)	0.047	LDA+U(1.0)	0.080
12.	PBEsol	0.064	PBEsol	0.088
13.	LDA	0.153	LDA	0.113

Variations in total magnetic moment across the transition can be probed by calculating the absolute magnetization via Eq. (7) for both the M1 and R phases. In Fig. 2 we show how the absolute magnetization $M = \int |\rho^{\uparrow} - \rho^{\downarrow}| dV$ changes as one selects among the available theoretical methods. The vertical gray line separates results calculated with PAW (VASP) and OPT (Quantum Espresso) potentials. Results for the M1 and R phases of VO_2 are represented by blue circles and red squares, respectively. A key property we observe is that the total magnetic moment–which is concentrated primarily on the V sites– remains essentially unchanged at about $1.1\mu_{\rm B}$ across the M1/R transition. This result is indicated by the horizontal dashed lines in Fig. 2.

In DFT the total magnetic moment is very sensitive to the functional employed and we observe two features of general interest in the data. First, as we ascend the "Jacob's ladder" of functionals (from local functionals to hybrids), we observe the total magnetic moment approaching the DMC benchmark values for each structural phase. Hybrid functionals and Hubbard corrected functionals (for selected values of U) attain almost total agreement with DMC on this measure. Second, and perhaps more interesting, functionals that most underestimate the magnetic moment in the R phase show increasingly greater imbalance toward demagnetization in the M1 phase.

This can be interpreted as a direct reflection of the degree of self-interaction error present in a given functional. Self-interaction error relates to the lack of preferential localization of charge on separated atoms. In both phases, the vanadium atoms are arranged on effectively one dimensional chains. In the R phase, the V atoms are equidistant and we might expect that functionals with a larger self-interaction error will tend to delocalize charge across the neighboring V sites. In the AFM state, neighboring atoms contain localized 3d charge of opposing spin, and so the charge delocalization leads to a reduction in the local magnetic moment. This effect is enhanced in the M1 phase, where the primary structural change is that the V atoms are no longer equidistant but dimerize, forming pairs. This increase in proximity leads to further erroneous charge sharing and hence a stronger shift toward demagnetization. Along these lines, we should note that among the non-hybrids the recently developed SCAN functional stands out as remaining nearly balanced in terms of magnetization across the transition. This is consistent with the notion that the enforcement of the known exact constraints on the functional has effectively reduced, though not eliminated, self-interaction error.

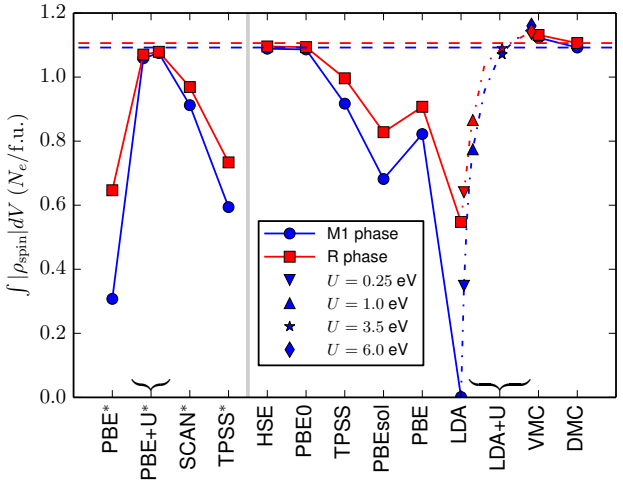

FIG. 2. Magnetization $M = \int |\rho^{\uparrow} - \rho^{\downarrow}| dV$ in units of N_e/formula unit from different methods for the two considered phases: M1 (blue) and R (red). The asterisk symbol refers to PAW results with VASP, where the U-values are 3.5 eV (left), and 4.0 eV (right). The other results are obtained with hard norm conserving pseudopotential (OPT) using Quantum Espresso. For the DMC values we have used the spin density from the extrapolated estimator.

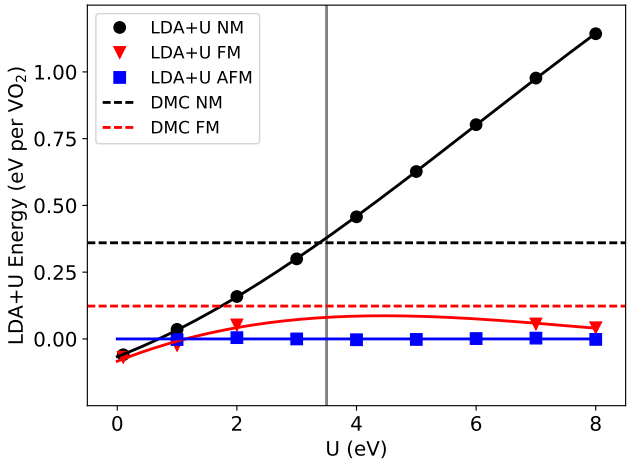

FIG. 3. LDA+U spin gap as a function of U for M1 VO_2. The energy of the ferromagnetic (FM) and fully spin unpolarized (or non-magnetic, NM) states are shown relative to the antiferromagnetic (AFM) state. Cubic fits to the data–performed prior to referencing against AFM–are shown as solid lines. Dashed lines correspond to the DMC results from Ref. 18. Ferromagnetic calculations in the range $U = 2 - 6$ eV were unstable.

It is also interesting to consider the relationship between spin density quality and the reproduction of reference spin gaps. With the OPT-potentials and LDA+U we performed a spin gap study as a function of U, where we consider the energy differences in the M1 phase between AFM, ferromagnetic (FM), and non-magnetic (NM) orderings. This is shown in Fig. 3 where we compare LDA+U results with different U-values (solid symbols) to DMC[18] (horizontal dashed lines). The vertical gray line marks the location of the optimal U value according to the variational DMC total energy. For this U value, the LDA+U results ($E_{\rm FM-AFM} \sim 80$ meV (estimated), $E_{\rm NM-AFM} = 380$ meV) are quite similar to the DMC spin gap values and it is also at this point that the LDA+U magnetic moment is correct (See Fig. 3). As HSE also gets the magnetic moment close to correct, we compare to previously calculated spin gaps. In Ref.[89] the FM-AFM difference is found to be 102 meV with the non-magnetic state (NM-AFM) residing at 463 meV. For comparison the DMC values[18] are $E_{\rm FM-AFM} = 123(6)$ meV and $E_{\rm NM-AFM} \approx 360$ meV. Unlike total energies and densities, these results suggest a close connection between the quality of spin energetics and spin densities in VO_2 for current generation functionals.

In general, many functionals have in common the challenges related to strongly correlated systems, e.g., increased self-interaction error arising from the localized 3d orbitals. Currently, these challenges can be tuned to some extent, e.g., by an "optimized" U, which requires external information to determine. Optimizing the U-parameter seems to have a clear correlation to improving the accuracy in modeling the magnetic properties, however, within the density functional theory framework this does not relate to improvements in the formation energy. The most common consequence of a poorly ranked functional is that even if one property can be obtained relatively accurately, obtaining reliable conclusions on other properties is not guaranteed. For example, predicting energetically the correct ground state structure does not imply that magnetic properties or phase stability would be described reliably. Overall, an accurate account of both the energy and density remains elusive as functionals that show the closest fidelity to either energetics (the meta-GGA's) or the (spin) density (hybrids and tuned LDA+U) generally retain significant room for improvement in the description of electronic correlation evident in both areas. Therefore, we hope that the extensive data we provide will be efficiently utilized in developing functionals that can capture all the properties reliably.

IV. CONCLUSIONS

In this work we used the diffusion Monte Carlo method as a reference in comparing properties related to phase stability and magnetism in vanadium dioxide within density functional theory using current generation functionals ascending "Jacob's ladder". The main focus was directed on antiferromagnetic VO_2 in M1 and R phases, for which our local and global metrics based on energetics, total density and spin density address the limitations in the description of correlated 3d orbital physics present in currently available density functionals. As in the recent

study for atoms by Medvedev et al.[24], we also come to the conclusion that the best match regarding total energies does not necessarily connect with the best match in the electron density.

In terms of phase stability, functionals which predicted the correct zero temperature structure (the M1 phase) showed mixed performance in terms of the total charge density. We do however find evidence that accurate spin densities are related to obtaining correct energy orderings of magnetic states. The density functionals surveyed displayed a wide variation in the calculated V-site magnetic moment–generally tending toward demagnetization–which can be reconciled in terms of self-interaction error.

Our work provides accurate energetics, charge and spin densities which serve as important benchmarks for future functional development both in general and especially in addressing the challenges related to the description of correlated 3d orbital physics within transition metal oxides. Importantly, our benchmark/reference data enables the accuracy of both the energy and the electron density to be monitored simultaneously, which is useful for functional development towards an exchange-correlation functional with exact properties. So far, this kind of detailed high accuracy reference data for correlated materials–for which VO_2 may be viewed as a prototype– has been absent from the literature. Due to the noticeable challenges arising from self-interaction error and description of 3d orbitals we believe our reference data has potential to enable improvements in future density functionals.

V. ACKNOWLEDGMENTS

This work was supported by the U.S. Department of Energy, Office of Science, Basic Energy Sciences, Materials Sciences and Engineering Division, as part of the Computational Materials Sciences Program and Center for Predictive Simulation of Functional Materials. This research used resources of the Oak Ridge Leadership Computing Facility at the Oak Ridge National Laboratory, which is supported by the Office of Science of the U.S. Department of Energy under Contract No. DE-AC05-00OR22725.

† kylanpaait@ornl.gov

[1] S. Lee, K. Hippalgaonkar, F. Yang, J. Hong, C. Ko, J. Suh, K. Liu, K. Wang, J. J. Urban, X. Zhang, C. Dames, S. A. Hartnoll, O. Delaire, and J. Wu, Science **355**, 371 (2017).
[2] Y. Chen, S. Zhang, F. Ke, C. Ko, S. Lee, K. Liu, B. Chen, J. W. Ager, R. Jeanloz, V. Eyert, and J. Wu, Nano Letters **17**, 2512 (2017).
[3] D. Y. Lei, K. Appavoo, F. Ligmajer, Y. Sonnefraud, R. F. Haglund, and S. A. Maier, ACS Photonics **2**, 1306 (2015).
[4] W. A. Vitale, M. Tamagnone, N. Émond, B. L. Drogoff, S. Capdevila, A. Skrivervik, M. Chaker, J. R. Mosig, and A. M. Ionescu, Scientific Reports **7**, 41546 (2017).
[5] W. A. Vitale, E. A. Casu, A. Biswas, T. Rosca, C. Alper, A. Krammer, G. V. Luong, Q.-T. Zhao, S. Mantl, A. Schüler, and A. M. Ionescu, Scientific Reports **7**, 355 (2017).
[6] D. W. Ferrara, J. Nag, E. R. MacQuarrie, A. B. Kaye, and R. F. Haglund, Nano Letters **13**, 4169 (2013).
[7] J. Holleman, M. M. Bishop, C. Garcia, J. S. R. Vellore Winfred, S. Lee, H. N. Lee, C. Beekman, E. Manousakis, and S. A. McGill, Phys. Rev. B **94**, 155129 (2016).
[8] J. D. Budai, J. Hong, M. E. Manley, E. D. Specht, C. W. Li, J. Z. Tischler, D. L. Abernathy, A. H. Said, B. M. Leu, L. A. Boatner, R. J. McQueeney, and O. Delaire, Nature **515**, 535 (2014).
[9] F. J. Morin, Phys. Rev. Lett. **3**, 34 (1959).
[10] A. Tselev, I. A. Lukyanchuk, I. N. Ivanov, J. D. Budai, J. Z. Tischler, E. Strelcov, A. Kolmakov, and S. V. Kalinin, Nano Letters **10**, 4409 (2010).
[11] M. A. Huber, M. Plankl, M. Eisele, R. E. Marvel, F. Sandner, T. Korn, C. Schller, R. F. Haglund, R. Huber, and T. L. Cocker, Nano Letters **16**, 1421 (2016).
[12] M. Imada, A. Fujimori, and Y. Tokura, Rev. Mod. Phys. **70**, 1039 (1998).
[13] Z. Zhang, F. Zuo, C. Wan, A. Dutta, J. Kim, J. Rensberg, R. Nawrodt, H. H. Park, T. J. Larrabee, X. Guan, Y. Zhou, S. M. Prokes, C. Ronning, V. M. Shalaev, A. Boltasseva, M. A. Kats, and S. Ramanathan, Phys. Rev. Applied **7**, 034008 (2017).
[14] A. Zylbersztejn and N. F. Mott, Phys. Rev. B **11**, 4383 (1975).
[15] V. Eyert, Annalen der Physik **11**, 650 (2002).
[16] Z. Zhu and U. Schwingenschlögl, Phys. Rev. B **86**, 075149 (2012).
[17] O. Nájera, M. Civelli, V. Dobrosavljević, and M. J. Rozenberg, Phys. Rev. B **95**, 035113 (2017).
[18] H. Zheng and L. K. Wagner, Phys. Rev. Lett. **114**, 176401 (2015).
[19] P. Hohenberg and W. Kohn, Phys. Rev. **136**, B864 (1964).
[20] W. Kohn and L. Sham, Phys. Rev. **140**, A1133 (1965).
[21] K. Appavoo, B. Wang, N. F. Brady, M. Seo, J. Nag, R. P. Prasankumar, D. J. Hilton, S. T. Pantelides, and R. F. Haglund, Nano Letters **14**, 1127 (2014).
[22] B. Xiao, J. Sun, A. Ruzsinszky, and J. P. Perdew, Phys. Rev. B **90**, 085134 (2014).

[23] H. Wang, T. A. Mellan, R. Grau-Crespo, and U. Schwingenschlögl, Chem. Phys. Lett. **608**, 126 (2014).
[24] M. G. Medvedev, I. S. Bushmarinov, J. Sun, J. P. Perdew, and K. A. Lyssenko, Science **355**, 49 (2017).
[25] W. M. C. Foulkes, L. Mitas, R. J. Needs, and G. Rajagopal, Rev. Mod. Phys. **73**, 33 (2001).
[26] N. M. Tubman, I. Kylänpää, S. Hammes-Schiffer, and D. M. Ceperley, Phys. Rev. A **90**, 042507 (2014).
[27] Y. Yang, I. Kylänpää, N. M. Tubman, J. T. Krogel, S. Hammes-Schiffer, and D. M. Ceperley, J. Chem. Phys. **143**, 124308 (2015).
[28] C. J. Umrigar, M. P. Nightingale, and K. J. Runge, J. Chem. Phys. **99**, 2865 (1993).
[29] J. B. Anderson, J. Chem. Phys. **63**, 1499 (1975).
[30] D. M. Ceperley and B. J. Alder, Phys. Rev. Lett. **45**, 566 (1980).
[31] L. K. Wagner and D. M. Ceperley, Rep. Prog. Phys. **79**, 094501 (2016).
[32] L. K. Wagner, J. Phys.: Condens. Matter **19**, 343201 (2007).
[33] J. Kolorenč and L. Mitas, Phys. Rev. Lett. **101**, 185502 (2008).
[34] L. Mitas and J. Kolorenč, Reviews in Mineralogy and Geochemistry **71**, 137 (2010).
[35] J. Kolorenč, S. Hu, and L. Mitas, Phys. Rev. B **82**, 115108 (2010).
[36] K. Foyevtsova, J. T. Krogel, J. Kim, P. R. C. Kent, E. Dagotto, and F. A. Reboredo, Phys. Rev. X **4**, 031003 (2014).
[37] L. K. Wagner and P. Abbamonte, Phys. Rev. B **90**, 125129 (2014).
[38] J. Yu, L. K. Wagner, and E. Ertekin, J. Chem. Phys. **143**, 224707 (2015).
[39] Y. Luo, A. Benali, L. Shulenburger, J. T. Krogel, O. Heinonen, and P. R. C. Kent, New Journal of Physics **18**, 113049 (2016).
[40] J. A. Santana, J. T. Krogel, P. R. C. Kent, and F. A. Reboredo, J. Chem. Phys. **144**, 174707 (2016).
[41] A. Benali, L. Shulenburger, J. T. Krogel, X. Zhong, P. R. C. Kent, and O. Heinonen, Phys. Chem. Chem. Phys. **18**, 18323 (2016).
[42] K. Doblhoff-Dier, J. Meyer, P. E. Hoggan, G.-J. Kroes, and L. K. Wagner, J. Chem. Theory Comput. **12**, 2583 (2016).
[43] J. P. Perdew and A. Zunger, Phys. Rev. B **23**, 5048 (1981).
[44] J. P. Perdew, K. Burke, and M. Ernzerhof, Phys. Rev. Lett. **77**, 3865 (1996).
[45] J. P. Perdew, K. Burke, , and M. Ernzerhof, Phys. Rev. Lett. **78**, 1396 (1997).
[46] J. P. Perdew, A. Ruzsinszky, G. I. Csonka, O. A. Vydrov, G. E. Scuseria, L. A. Constantin, X. Zhou, and K. Burke, Phys. Rev. Lett. **100**, 136406 (2008).
[47] J. P. Perdew, A. Ruzsinszky, G. I. Csonka, O. A. Vydrov, G. E. Scuseria, L. A. Constantin, X. Zhou, and K. Burke, Phys. Rev. Lett. **102**, 039902(E) (2009).
[48] J. Tao, J. P. Perdew, V. N. Staroverov, and G. E. Scuseria, Phys. Rev. Lett. **91**, 146401 (2003).
[49] J. Sun, A. Ruzsinszky, and J. P. Perdew, Phys. Rev. Lett. **115**, 036402 (2015).
[50] J. Sun, R. C. Remsing, Y. Zhang, Z. Sun, A. Ruzsinszky, H. Peng, Z. Yang, A. Paul, U. Waghmare, X. Wu, M. L. Klein, and J. P. Perdew, Nature Chem. **8**, 831 (2016).
[51] J. P. Perdew, M. Ernzerhof, and K. Burke, J. Chem. Phys. **105**, 9982 (1996).
[52] J. Heyd, G. E. Scuseria, and M. Ernzerhof, J. Chem. Phys. **118**, 8207 (2003).
[53] J. Heyd, G. E. Scuseria, and M. Ernzerhof, J. Chem. Phys. **124**, 219906 (2006).
[54] V. I. Anisimov, J. Zaanen, and O. K. Andersen, Physical Review B **44**, 943 (1991).
[55] A. M. Rappe, K. M. Rabe, E. Kaxiras, and J. D. Joannopoulos, Phys. Rev. B **41**, 1227 (1990).
[56] G. Kresse and J. Hafner, Phys. Rev. B **47**, 558 (1993).
[57] G. Kresse and J. Hafner, Phys. Rev. B **49**, 14251 (1994).
[58] G. Kresse and J. Furthmüller, Comput. Mat. Sci. **6**, 15 (1996).
[59] G. Kresse and J. Furthmüller, Phys. Rev. B **54**, 11169 (1996).
[60] P. E. Blochl, Phys. Rev. B **50**, 17953 (1994).
[61] G. Kresse and D. Joubert, Phys. Rev. B **59**, 1758 (1999).
[62] P. Giannozzi, S. Baroni, N. Bonini, M. Calandra, R. Car, C. Cavazzoni, D. Ceresoli, G. L. Chiarotti, M. Cococcioni, I. Dabo, A. Dal Corso, S. de Gironcoli, S. Fabris, G. Fratesi, R. Gebauer, U. Gerstmann, C. Gougoussis, A. Kokalj, M. Lazzeri, L. Martin-Samos, N. Marzari, F. Mauri, R. Mazzarello, S. Paolini, A. Pasquarello, L. Paulatto, C. Sbraccia, S. Scandolo, G. Sclauzero, A. P. Seitsonen, A. Smogunov, P. Umari, and R. M. Wentzcovitch, J. Phys.: Condensed Matter **21**, 395502 (2009).
[63] K. F. Garrity, J. W. Bennett, K. M. Rabe, and D. Vanderbilt, Computational Materials Science **81**, 446 (2014).
[64] J. T. Krogel, Comput. Phys. Commun. **198**, 154 (2016).
[65] J. Longo and P. Kierkegaard, Acta Chemica Scandinavica **24**, 420 (1970).
[66] M. Ghedira, H. Vincent, M. Marezio, and J. Launay, J. Solid State Chem. **22**, 423 (1977).
[67] M. Hellenbrandt, Crystallography Reviews **10**, 17 (2004).
[68] *Supplemental Material*.
[69] J. Kim, K. P. Esler, J. McMinis, M. A. Morales, B. K. Clark, L. Shulenburger, and D. M. Ceperley, J. Phys. Conf. Ser. **402**, 012008 (2012).
[70] C. Lin, F. H. Zong, and D. M. Ceperley, Phys. Rev. E **64**, 016702 (2001).
[71] J. C. Slater, Phys. Rev. **34**, 1293 (1929).
[72] R. Jastrow, Phys. Rev. **98**, 1479 (1955).
[73] N. D. Drummond, M. D. Towler, and R. J. Needs, Phys. Rev. B **70**, 235119 (2004).
[74] C. J. Umrigar, J. Toulouse, C. Filippi, S. Sorella, and R. G. Hennig, Phys. Rev. Lett. **98**, 110201 (2007).
[75] M. M. Hurley and P. A. Christiansen, J. Chem. Phys. **86**, 10691070 (1987).
[76] L. Mitas, E. L. Shirley, and D. M. Ceperley, J. Chem. Phys. **95**, 34673475 (1991).
[77] M. Casula, Phys. Rev. B **74**, 161102 (2006).
[78] C. J. Umrigar and C. Filippi, Phys. Rev. Lett. **94**, 150201 (2005).
[79] J. B. Anderson, J. Chem. Phys. **63**, 1499 (1975).
[80] J. B. Anderson, J. Chem. Phys. **65**, 4121 (1976).
[81] G. Ortiz, D. M. Ceperley, and R. M. Martin, Phys. Rev. Lett. **71**, 2777 (1993).
[82] M. Casula, C. Filippi, and S. Sorella, Phys. Rev. Lett. **95**, 100201 (2005).
[83] B. Blaiszik, K. Chard, J. Pruyne, R. Ananthakrishnan, S. Tuecke, and I. Foster, JOM **68**, 2045 (2016).
[84] W. Kohn, Rev. Mod. Phys. **71**, 1253 (1999).
[85] J. A. Pople, Rev. Mod. Phys. **71**, 1267 (1999).
[86] J. A. Santana, J. T. Krogel, J. Kim, P. R. C. Kent, and F. A. Reboredo, J. Chem. Phys. **142**, 164705 (2015).

[87] C. Mitra, J. T. Krogel, J. A. Santana, and F. A. Reboredo, J. Chem. Phys. **143**, 164710 (2015).
[88] J. A. Santana, J. T. Krogel, P. R. C. Kent, and F. A. Reboredo, J. Chem. Phys. **147**, 034701 (2017).
[89] R. Grau-Crespo, H. Wang, and U. Schwingenschlögl, Phys. Rev. B **86**, 081101 (2012).